Role of Charge Distribution in the Reactant and Product in Double Layer Effects: Construction of Corrected Tafel Plots

Maria Yu. Rusanova,[†] Galina A. Tsirlina,[‡] Renat R. Nazmutdinov,[§] and W. Ronald Fawcett*,[†]

Department of Chemistry, University of California, Davis, California 95616, Chemical Faculty, Moscow State University, Moscow 119899, Russia, and Kazan State Technological University, Kazan 420015, Russia

Received: July 12, 2004; In Final Form: October 11, 2004

The effect of charge distribution within Cr(III) and Eu(III) aquacomplexes on the kinetics of simple electron-transfer reactions at electrodes is considered. The construction of corrected Tafel plots using noninteger effective charges for the reactant and product estimated on the basis of quantum-chemical data was shown to be more reasonable than the traditional approach in which integer charges are assumed. The potential distribution near the electrode has been estimated both by the Gouy−Chapman model and from Monte Carlo simulations for 1−1 supporting electrolytes. Kinetic parameters obtained using the two approaches are compared.

Introduction

The construction of corrected Tafel plots (cTp)[1,2] has remained the most widely used approach to the analysis of experimental data for electrochemical kinetics. Generally, the Frumkin correction is involved with the assumption that the reactant is a point charge located at the outer Helmholtz plane (oHp). In addition, it is usual to assume that the structure of the diffuse double layer is described by the Gouy−Chapman model. Application of this approach to the analysis of experimental data was most successful for the case of anion reduction at negatively charged electrodes,[2] that is for very strong repulsion of the reactant by the electrode's field.

To construct a cTp the experimental dependence of the rate constant k_f on the electrode potential is usually plotted as ($\ln k_f + z_A f\phi^d$) against ($\phi^m - \phi^d$), where z_A is the charge on the reacting species, $f = F/RT$ (F, R, and T have their usual meaning), ϕ^d is the potential at the oHp and ϕ^m is the rational potential ($\phi^m = E - E_z$ where E is the experimental potential and E_z is the zero charge potential).

The role of charge distribution in the reactant and product species in the kinetics of electrochemical reactions has been discussed in a series of recent papers.[3−5] It has been found that the magnitude of the double layer correction is affected by the atomic charge distribution in metal complexes undergoing simple heterogeneous electron transfer reactions. On the basis of quantum chemical calculations for redox couples involving cobalt and iron complexes and a simple model for the interfacial potential drop, it was shown that the double layer effect is mainly determined by the charge and geometry of the ligands.[4] With a molecular level reconsideration of the work terms, it was proposed that the double layer effect may be described in terms of the effective charge z_e for the reactant (z_{Ae}) and product (z_{Be}). The effective charge of either species is defined as

$$z_e = \frac{\sum z_i \phi^i}{\phi^d} \qquad (1)$$

where z_i is the local charge on an atom or group of atoms comprising the complex, and ϕ^i is the potential at the corresponding site. The value of z_e for an asymmetrical species, which can reorient in the electrical field due to its dipole moment, is generally found to depend on the electrode charge density and the concentration of the supporting electrolyte. In summary, z_e can be regarded as the charge of a hypothetical reactant with no volume which experiences the potential on the oHp, ϕ^d.

In earlier[6] work, various integer values of the reactant charge, z_A, were applied to construct cTps for the case of the reduction of hexaamminecobalt (III) on gold single crystals with low Miller indices. The difference between the bulk charge value of the nonassociated reactant (+3) and the value of z_A, for which the cTps for different surface crystallographic orientations of Au overlap and approach linearity (+2) was explained by the formation of ion pairs in the bulk of the solution. Until now, it has not been verified how the approach based on determining z_e of the reactant and product, and thus, the application of noninteger charge values could be used in the construction of cTps.

In this paper, the kinetics of reduction of europium(III) and chromium(III) aquacomplexes in an acidic medium on mercury is analyzed using a modified approach for cTp construction. These two cationic complexes with similar general geometries, but different bond lengths and inner charge distributions undergo a simple one-electron reduction at a negatively charged mercury surface. Application of the effective charge z_e with both integer and noninteger values for the construction of cTps for these reactions is shown below to allow one to come to a reasonable understanding of the role of specific molecular features in the interaction of the reacting couple with the field of the electrode.

The accuracy of the z_e estimation is determined by the selection of a model for the potential distribution in the vicinity of the electrode surface. Previously, the Gouy−Chapman model was widely used in order to explain double layer effects on the kinetics of electrochemical reactions.[1] In this regard, the potential distribution perpendicular to the electrode/solution interface plays a key role in the estimation of z_e. When the reacting complex has a size comparable with the Debye length, the assumptions of the Gouy−Chapman model can cause some misinterpretation in the data analysis. Therefore, in this paper,

[†] University of California, Davis.
[‡] Moscow State University.
[§] Kazan State Technological University.

10.1021/jp046917s CCC: $30.25
Published on Web 01/27/2005

an alternative model of the diffuse layer which recognizes finite ion size and which is based on Monte Carlo simulations is also applied to determine the interfacial potential distribution.[7]

Experimental Section

A conventional three-electrode glass cell with glass ground joints was used for all the experiments. It should be emphasized that in cases when the solution has to be oxygen-free, some standard commercially available cells which cannot be sealed from the atmosphere are not suitable. In the case of chromium(III) containing solutions, the reaction between the residual oxygen and the product of $[Cr(H_2O)_6]^{3+}$ reduction, namely, the Cr(II) aquacomplex, may yield superoxochromium(III) ion.[8−10] Reduction of this ion can significantly complicate the kinetic results and make their interpretation impossible.

The working electrode was a hanging drop mercury electrode (controlled growth mercury electrode manufactured by BAS). The saturated calomel reference electrode and platinum counter electrode completed the three-electrode setup. The cleanliness of the supporting electrolyte solutions was verified by cyclic voltammetry. To minimize contamination of the working solutions with chloride ions and decrease the value of the liquid junction potential, the reference electrode was connected to the cell through a Luggin capillary filled with a 0.5 M $NaClO_4$ solution.

All solutions were prepared with Nanopure water with a minimum resistivity of 18 MΩ/cm (Barnstead). Glassware was cleaned in boiling 50% nitric acid or in a mixture of concentrated nitric and hydrochloric acids (1:3) and washed with Nanopure water before each set of experiments. Perchloric acid, europium(III) perchlorate (40% aqueous solution, Aldrich), sodium perchlorate, and chromium(III) perchlorate hexahydrate (GFS Chemicals) were of the best quality available. If it was necessary, the salts were additionally dried.

The working solutions were thoroughly deaerated with high-purity argon moisturized before coming to the cell by bubbling through Nanopure water. For the cell used which had a volume of 50 mL, the deaeration time was 45−60 min. During the experiments an argon atmosphere was maintained above the working solution.

Cyclic voltammograms (CVs) were obtained by using a Princeton Applied Research (PAR) 173 potentiostat with a PAR 175 universal programmer. The data were collected in digitized form by using a PowerLab/4S four-channel analyzer (AD Instruments) or by using the PAR 175 and a computer with a GPIB standard interface. The irreversible one-electron reduction of $[Eu(H_2O)_n]^{3+}$ and $[Cr(H_2O)_6]^{3+}$ ions in acidic (10^{-3} M $HClO_4$) solutions of $NaClO_4$ (0.03 and 0.3 M) was studied by cyclic voltammetry at a scan rate of 50 mV s^{-1}. In the case of chromium(III) solutions, it was important to maintain a pH of 3 to prevent hydrolysis of the complex.[11,12] Due to the fact that the reactions are sufficiently irreversible,[13,14] the contribution of the back anodic reaction was not taken into consideration. It was also assumed that specific adsorption of ClO_4^- ion is negligibly small in the studied potential range. Double layer capacity data were taken from the literature.[15] The potential of zero charge (E_z) was determined from the minimum current observed on a CV obtained in a 10^{-4} M solution of $HClO_4$. The value of E_z is in good agreement with literature data.[1] All the potentials are corrected for liquid junction potentials using the Henderson equation and are given on the saturated calomel electrode scale. The reduction current was also corrected for the charging current.

From the experimentally obtained CV data, after correction for the charging current, the rate constants were calculated for a totally irreversible reduction process using the expression

$$\ln k_f = -\ln\left[\frac{I_{lim} - I(t)}{i(t)}\right] + \ln D_A^{1/2} \qquad (2)$$

where $I(t)$ is the semiintegral of the measured current $i(t)$, I_{lim} is the limiting current, and D_A is the diffusion coefficient of the reacting species calculated using the expression

$$D_A^{1/2} = \frac{I_{lim}}{FAc_o} \qquad (3)$$

Here A is the effective surface area of the working electrode, and c_A is the concentration of the reactant.[15]. The semiintegration procedure was carried out as described in the literature.[16−18]

For all experiments, a freshly prepared working solution (5×10^{-4} M) of $Cr(H_2O)_6(ClO_4)_3$ or $Eu(H_2O)_6(ClO_4)_3$ was used. Between the experiments the working solutions were kept in the dark at a constant temperature of 25 °C. The experiments were carried out at a constant temperature of 25 °C.

The effective surface of the hanging drop mercury electrode was kept constant (0.024 ± 0.001 cm^2).

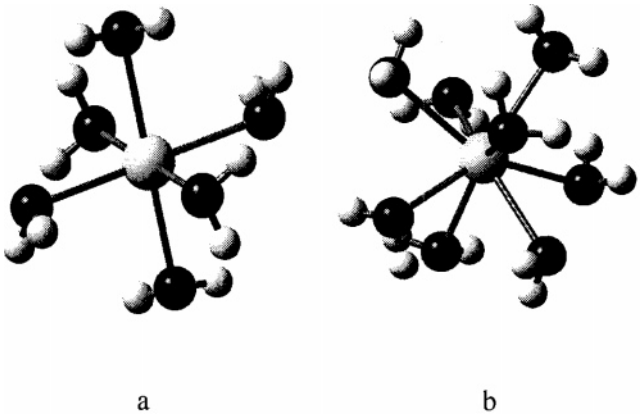

Figure 1. Structure of $[Eu(H_2O)_6]^{3+}$ or $[Cr(H_2O)_6]^{3+}$ (a) and $[Eu(H_2O)_8]^{3+}$ (b) ion complexes.

Computational Section

A. Quantum Chemical Calculations. The electronic structure of $[Cr(H_2O)_6]^{3+}$ and $[Cr(H_2O)_6]^{2+}$ complexes was fully treated at the density functional theory (DFT) level by the use of the B3LYP hybrid functional.[19] A six-coordinated octahedron structure ($T_{2g}^3E_g$) was assumed for $[Cr(H_2O)_6]^{3+}$ (Figure 1) which is in accordance with the X-ray diffraction (XRD) data.[20] The geometry of the aquacomplexes was optimized with some symmetry restrictions. A basis set of DZ quality was used to describe the valence electrons in the Cr atom.[21] The inner electrons were included in the relativistic Effective Core Potential (LanL2) developed by Hay and Wadt.[21] The standard basis set 6-311g(d, p) was employed to describe the electrons of the O and H atoms. A value of 201.5 pm was obtained for the Cr−O distance in the $[Cr(H_2O)_6]^{3+}$ complex, which is in a good agreement with the experimental data (198 pm[20]). The reduced form of aquacomplex possesses significant distortion due to the Jahn−Teller effect (Table 1).

Experimental data for the structure of Eu(III) in aqueous solution is somewhat controversial.[22−24] As follows from the XRD data,[22] the Eu(III) and related cationic (Tb(III), Er(III) and Sm(III)) aquacomplexes are eight-coordinated. It was concluded[24] that Sm(III) and Eu(III) exist in equilibrium between

TABLE 1: Geometry and Atomic Charge Distribution (q) in the Complex

a. $[Cr(H_2O)_6]^{3+}$ and $[Cr(H_2O)_6]^{2+}$ Complexes

complex	total spin	r(Cr−O)/pm	r(O−H)/pm	∠Cr−O−H/deg	q(Cr)	q(O)	q(H)
$[Cr(H_2O)_6]^{3+}$	3/2	201.5	96.4	125.1	+2.12	−1.02	+0.58
$[Cr(H_2O)_6]^{2+}$	2	211.6[a]/236.2[b]	96.6	126.0[a]/127.2[b]	+1.79	−1.01[a]/−0.99[b]	+0.53[a]/+0.50[b]

b. $[Eu(H_2O)_6]^{3+}$ Complex

complex	total spin	r(Eu−O)/pm	r(O−H)/pm	∠Eu−O−H/deg	q(Eu)	q(O)	q(H)
$[Eu(H_2O)_6]^{3+}$	3	251.0	98	105	+1.36	−0.66/−0.63/−0.72	+0.48,+0.46/+0.49,+0.46/+0.45, 0.48

c. $[Eu(H_2O)_8]^{3+}$ Complex

complex	total spin	r(Eu−O)/pm	r(O−H)/pm	∠Eu−O−H/deg	q(Eu)	q(O)	q(H)
$[Eu(H_2O)_8]^{3+}$	3	251.0	98	105	+1.47	−0.66/−0.7/−0.73/−0.74	+0.4, +0.44/+0.45,+0.46/+0.47

[a] Equatorial disposition of atoms. [b] Axial disposition of atoms.

nine- and eight-coordinated forms in aqueous solutions. On the other hand, a six-coordinated structure for the Eu(III) aquacomplex was assumed by Marcus.[24] Bearing in mind that the hydration energy of Eu(III) is significantly lower[24] than that of Cr(III), one might assume some reduction in the coordination number for a Eu(III) aquacomplex in the vicinity of the metal/solution interface. Therefore, the structure of several Eu(III) aquacomplexes ($[Eu(H_2O)_n]^{3+}$, $n = 6, 7, 8, 9$) has been examined. Since the accurate treatment of the geometry and electronic structure of molecular systems containing f-elements is a challenging and complicated computational problem,[25] a simpler method was employed. The geometry of $[Eu(H_2O)_n]^{3+}$ complexes was fully optimized using the molecular mechanics method (MM+) as implemented in the Hyperchem 7.0 program package.[26] It should be noted that the molecular properties used in the MM+ force field parametrization are normally related to compounds in a stable oxidation state. Therefore, in the present case the results of such calculations can be attributed to the Eu(III) species.

For $[Eu(H_2O)_6]^{3+}$ molecular mechanics predicts an octahedral coordination (Figure 1a). In turn, a square antiprismatic geometry with equal ion-oxygen distances was found to be optimal for the eight-coordinated aquacomplex (Figure 1b). Such a structure is in qualitative agreement with the results of molecular dynamics simulations for Yb^{3+} in aqueous solution[27]. The Eu−O bond lengths were computed to be in the region of 251−252 pm and depend very slightly on the n value. A value of 245 pm was reported for the Eu−O bond length (mixed Eu(III) aquachlorocomplexes[22]). On the other hand, comparing the XRD data[22] for aqua- and aquachlorocomplexes of Tb(III), Er(III) and Sm(III), one may assume that this bond might be 1−2 pm shorter in $[Eu(H_2O)_8]^{3+}$. In any case, the computed distance of 250 pm seems to be in satisfactory agreement with experimental data.

Since the MM+ computational scheme does not provide a reliable description of the electrostatic potential, a set of single point calculations for the $[Eu(H_2O)_n]^{3+}$ complexes at the DFT-(B3LYP) level was performed as the next step using the equilibrium geometry obtained earlier on the basis of the MM+ method. The valence s, p, d and f shells of the Eu atom were described by the CEP-121g basis set, the effect of inner electrons being addressed using the Effective Core Potential.[28] The standard 6-311g(d, p) basis set was used to describe the electrons of O and H atoms. The high-spin electronic state ($4f^6$ with a spin multiplicity of 7) was found to be the ground state for all the Eu(III) aquacomplexes considered. This might result from the fact that the Eu−ligand interaction is mainly electrostatic so that the 4f orbitals are not strongly involved in the bonding.

According to the results of the molecular mechanics calculations a seven-coordinated structure for the Eu(III) aquacomplex is preferred, whereas the complexes with $n = 6$ and 8 have practically the same potential energy values. At the same time, according to the DFT results the hydration energy increases monotonically going from $[Eu(H_2O)_6]^{3+}$ to $[Eu(H_2O)_9]^{3+}$ (279.1, 256.1, 241.8, and 228.0 kJ mol^{-1}, respectively, per water molecule).

The DFT calculations for both the $Cr(H_2O)_6]^{3+/2+}$ and $Eu(H_2O)_n]^{3+}$ complexes were performed on the basis of the unrestricted formalism using the Gaussian 98 program package.[29] Although the B3LYP functional does not provide an adequate treatment of open shell d- and f-metal complexes, nevertheless it can be used for comparative studies. The atomic charges were computed within the framework of the ChelpG scheme,[30] which yields the best fit of the molecular potential (metallic radii values were employed in these calculations for the Cr and Eu atoms).

To estimate possible effective charges, comparative calculations were performed for $[Eu(H_2O)_6]^{3+}$ and $[Eu(H_2O)_8]^{3+}$. Despite some differences in the internal charge distribution, no crucial differences in the value of z_e calculated using eq 1 were found.

B. Potential Distribution in the Diffuse Layer. Within the framework of the Gouy−Chapman model, the distribution of the potential, ϕ^i in the vicinity of the electrode surface at $x_i > x_d$ (where $x_d = 0$ is the position of the oHp) is given by the formula

$$\phi^i = \frac{4}{f}\tanh^{-1}\left\{\tanh\left(\frac{f\phi^d}{4}\right)\exp(-\kappa x_i)\right\} \qquad (4)$$

where $f = F/RT$ and κ is the Debye−Huckel reciprocal distance.

Monte Carlo simulations have been carried out for the diffuse double layer for 1−1 electrolytes in the concentration range from 0.1 to 2 M, and for electrode charges (σ_m) between −5 and −40 μC cm^{-2} In addition, ion diameters of 200, 300, and 400 pm were considered with the solvent modeled as a dielectric continuum using the relative permittivity of pure water.[31] The potential profile in the diffuse layer was also determined in these simulations. The results of the simulations were examined within the context of the Fawcett−Henderson model of the diffuse layer.[32,33] As a result it was shown that

$$\phi^d(MC) = d_1\phi^d(GC) + d_3[\phi^d(GC)]^3 \qquad (5)$$

where ϕ^d(MC) is the potential at the oHp according to the MC simulation and ϕ^d(GC), the value according to the Gouy−Chapman model. The constants d_1 and d_3 are based on the MSA parameters η and Γ. η is the volume fraction which is defined

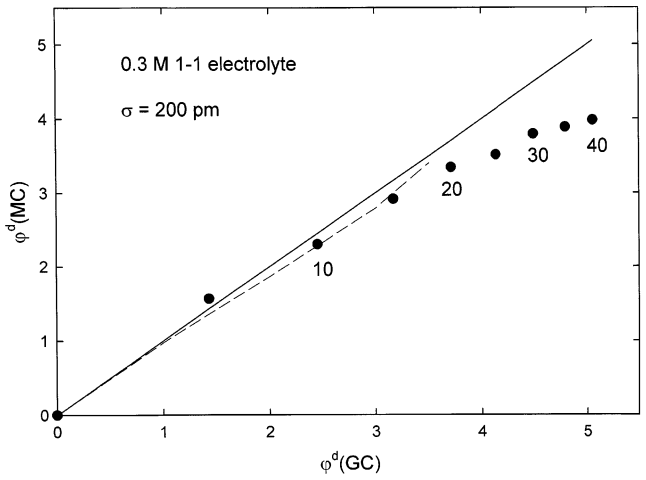

Figure 2. Plot of the dimensionless potential drop across the diffuse layer according to MC simulations, φ^{d}(MC), plotted against the same quantity estimated by the Gouy−Chapman model φ^{d}(GC). The integers indicate the electrode charge density in μC cm^{-2}. The curvature of the plot may be neglected for electrode charge densities less than 10 μC cm^{-2} as shown by the broken line through the first three points.

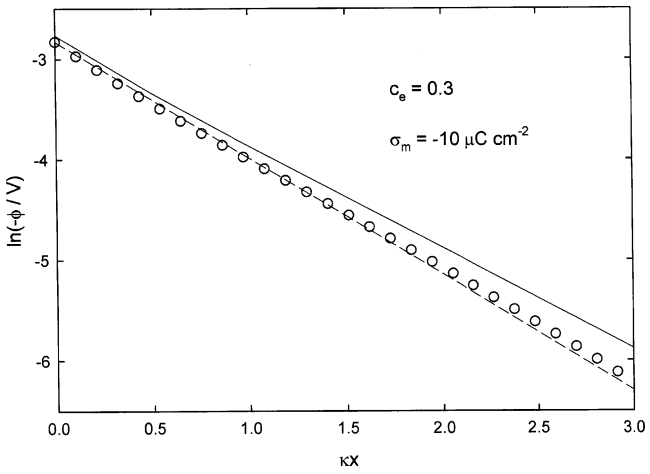

Figure 3. Plot of the logarithm of the potential in the diffuse layer against the distance parameter κx for a charge density of -10 μC cm^{-2} and electrolyte concentration of 0.3 M. The solid line shows the prediction of the GC model and the open circles the results of the MC simulation; the dotted line shows the MC results as estimated by eq 12.

from the theory of hard sphere fluids as

$$\eta = \frac{2000\pi N_{\mathrm{L}} c_{\mathrm{e}} \sigma^3}{6} \tag{6}$$

Here, N_{L} is the Avogadro constant, c_{e}, the base electrolyte concentration in M, and σ, the ion diameter. Γ is the relative value of the reciprocal distance in the MSA which characterizes the thickness of the ionic atmosphere around a given ion. It is defined by the equation

$$\Gamma = \frac{(1 + 2\sigma\kappa)^{1/2}}{2} - \frac{1}{2} \tag{7}$$

Typical results of the MC simulations for the case of an ion diameter of 200 pm and an electrolyte concentration of 0.3 M are shown in Figure 2. The broken line through the points was obtained by fitting eq 5 to the MC data. Analysis of MC results for five concentrations and three ion sizes leads to the conclusion that the parameters d_1 and d_3 are given by the equations

$$d_1 = \frac{1}{{a_0}^{1/2}} - \Gamma^2 \tag{8}$$

and

$$\mathrm{d}_3 = \frac{1}{24{a_0}^{1/2}} + \frac{\eta^{1/2}}{4{a_0}^{1/2}} - \frac{1}{{a_0}^{3/2}} - \frac{\Gamma^2}{24} - \frac{\Gamma}{8(1+\Gamma)} \tag{9}$$

Here, a_0 is the hard sphere compressibility given by

$$a_0 = \frac{(1 + \eta + \eta^2 - \eta^3)}{(1 - \eta)^3} \tag{10}$$

Furthermore, it is clear that the term in d_3 describing the curvature of the plot in Figure 2 can be neglected when the electrode charge density is less than 15 μC cm^{-2} at this ionic strength (0.3 M). This means that eqs 5−8 provide a very simple way of estimating ϕ^{d}(MC) for the present experiments.

The potential profile in the diffuse layer near the oHp was also examined from the simulation results. For the present experiments in which the magnitude of the charge density is not large, eq 4 simplifies to

$$\phi^{i}(\mathrm{GC}) = \phi^{\mathrm{d}}(\mathrm{GC}) \exp(-\kappa x_i) \tag{11}$$

where x_i is the distance from the oHp. In the case of the MC results, the potential profile is given by

$$\phi^{i}(\mathrm{MC}) = \phi^{\mathrm{d}}(\mathrm{MC}) \exp(-\kappa\sigma x_i/(2\Gamma)) \tag{12}$$

In this case the distance x_i is measured from the oHp in the MC simulation which occurs at 100 pm when the ion diameter is 200 pm. The dependence of potential on position in the diffuse layer is illustrated in Figure 3. It is clear that the potential drops more rapidly in the case of the MC data. As can be seen from the fit of the MC data, the slope of the plot of $\ln(-\phi)$ against κx is related to the same slope in the GC model by the ratio $\kappa\sigma/2\Gamma$ as one would expect from the MSA model.[32]

The potential of the outer Helmholz plane by the Gouy−Chapman model, ϕ^{d}(GC) was calculated by using the formula

$$\phi^{\mathrm{d}} = \frac{2}{f}\ln\left(\frac{\sigma_{\mathrm{m}}}{2A_{\mathrm{GC}}} + \sqrt{\frac{{\sigma_{\mathrm{m}}}^2}{4{A_{\mathrm{GC}}}^2} + 1}\right) \tag{13}$$

where σ_{m} is the charge density on the mercury. The constant A_{GC} is equal to $5.8687(I)^{1/2}$ in water at 25 °C where I is the ionic strength of the solution.

Results and Discussion

A typical dependence of the reduction current on the electrode potential for the reduction of $[Eu(H_2O)_n]^{3+}$ and $[Cr(H_2O)_6]^{3+}$ ions in an acidic (10^{-3} M $HClO_4$) solution of $NaClO_4$ (0.3 M) is presented in Figure 4, parts a and b. The fact that the limiting current is not constant can be explained by the contribution of hydrogen evolution from water molecules in the coordination sphere of the complex in that potential region. The values of the limiting current were assumed to correspond those of the region where the plateau begins.

One can see from the data in Figure 4 that Eu(III) reduction is slightly faster than that of Cr(III), and the diffusion coefficient for the Eu(III) species is higher than that of the Cr(III) species. The values of D_{A} calculated from the experimental data were as follows: for the Eu(III) complex, 6.1×10^{-6} and 6.7×10^{-6}

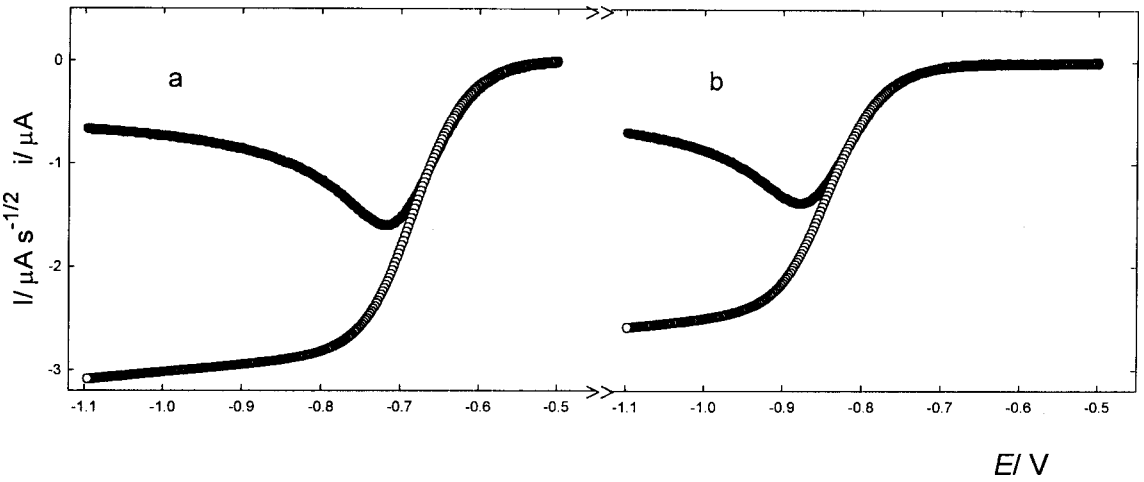

Figure 4. Typical current waves for the reduction of $[Eu(H_2O)_6]^{3+}$ (a) and $[Cr(H_2O)_6]^{3+}$ (b) ions (5×10^{-4} M) in a solution of 10^{-3} M $HClO_4$ + 0.3 M $NaClO_4$ (solid circles) and the corresponding semiintegrals (open circles).

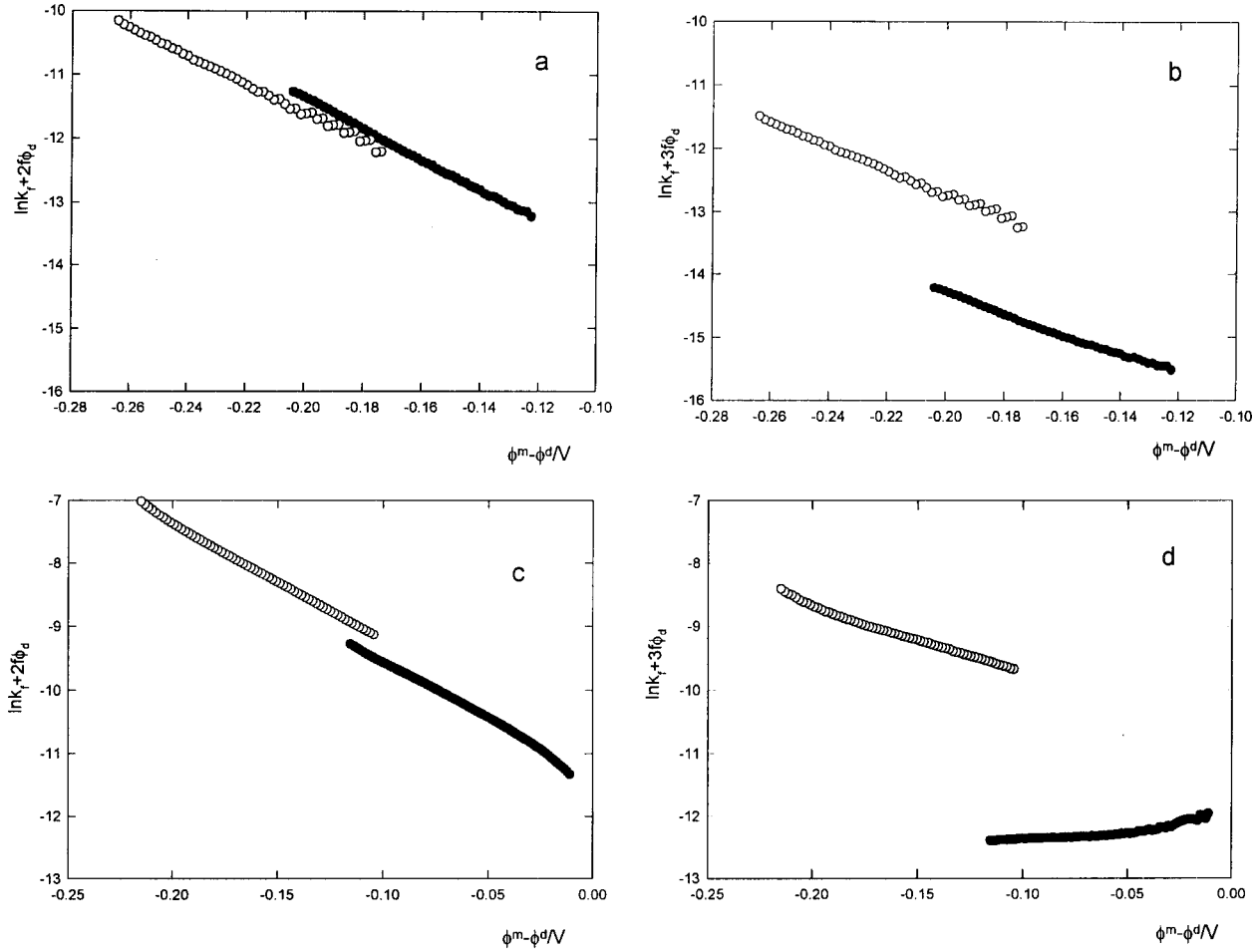

Figure 5. Corrected Tafel plots for the reduction of $[Cr(H_2O)_6]^{3+}$ (a, b) and $[Eu(H_2O)_n]^{3+}$ (c, d) ions (5×10^{-4} M) in a solution of 10^{-3} M $HClO_4$ with 0.3 M $NaClO_4$ (open circles) or with 0.03 M $NaClO_4$ (solid circles) for $z_A = +2$ (a, c) and $z_A = +3$ (b, d).

$cm^2\ s^{-1}$, and for the Cr(III) complex, 4.4×10^{-6} and 5.1×10^{-6} $cm^2\ s^{-1}$ in 0.3 M $NaClO_4$ + 10^{-3} M $HClO_4$ and 0.03 M $NaClO_4$ + 10^{-3} M $HClO_4$, respectively. The experimental data are in good agreement with the values of D_A found in the literature: for the aquo−Eu(III) complex ion (7.1×10^{-6} $cm^2\ s^{-1}$ is the average value for a set of solutions $NaClO_4$ + $HClO_4$ with different ionic strengths[14]) and for the aquo−Cr(III) complex ion (4.1×10^{-6} $cm^2\ s^{-1}$ in 0.51 M $NaClO_4$ + 0.01 M $HClO_4$[11]).

From the CVs and the semiintegrated data for the reduction of $[Cr(H_2O)_6]^{3+}$ in the two solutions (0.3 and 0.03 M $NaClO_4$ + 10^{-3} M $HClO_4$), the reduction rate constants were calculated using eq 2. The obtained values of the rate constants in 0.3M $NaClO_4$ + $HClO_4$ are in excellent agreement with data reported by Weaver and Anson,[34] where the experiments were carried out in the identical supporting electrolytes and with data for Eu(III) reduction presented by Gierst and Cornellisen[14] for less acidic supporting electrolyte. The calculated rate constants for

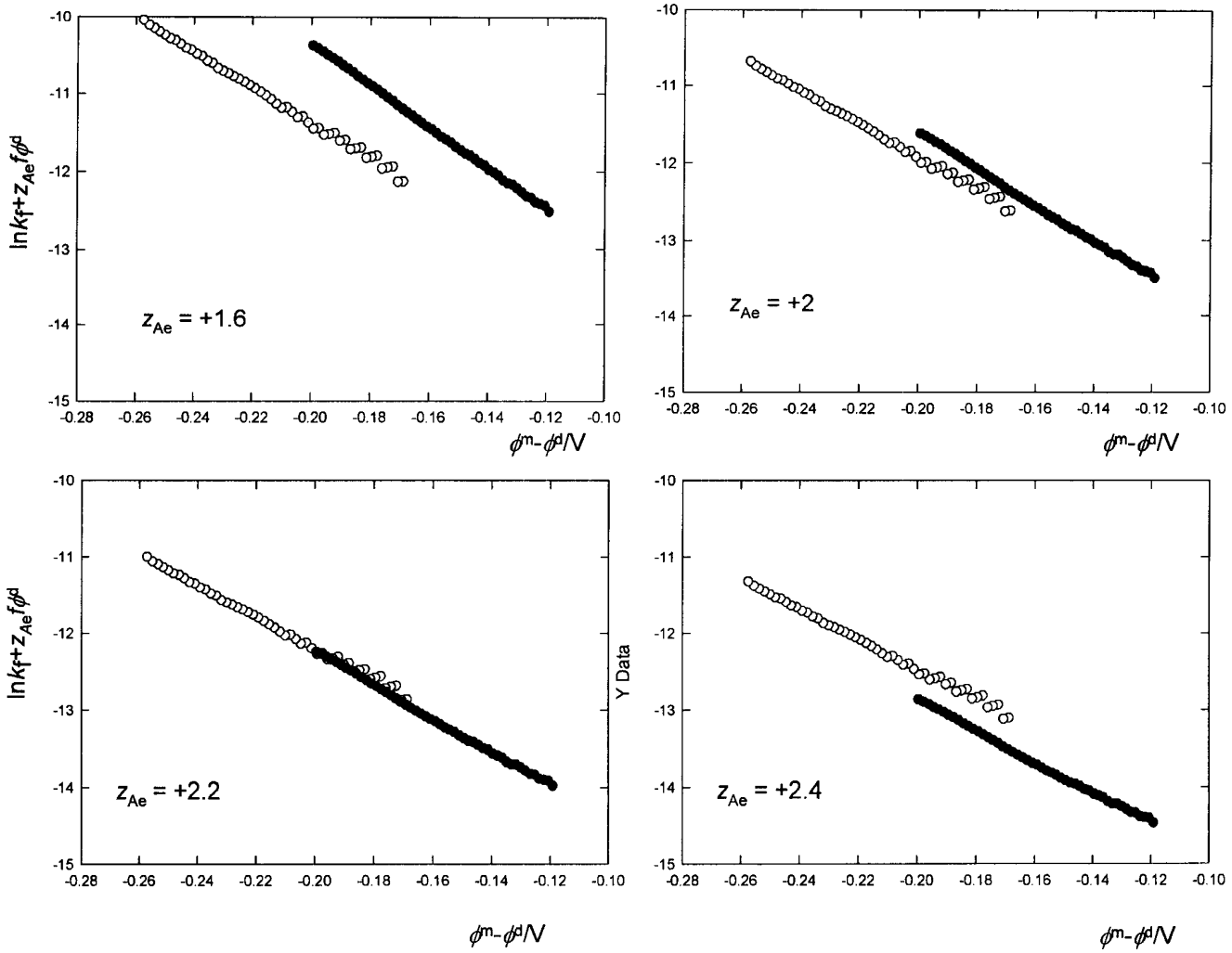

Figure 6. cTp for reduction of $[Cr(H_2O)_6]^{3+}$ ions (5×10^{-4} M) in a solution of 0.3M $NaClO_4$ + 10^{-3} $HClO_4$ (open circles) and 0.03M $NaClO_4$ + 10^{-3} $HClO_4$ (solid circles) for different effective charges of the reacting complex.

reduction of Eu(III) in 0.3M $NaClO_4$ + 10^{-3} M $HClO_4$ are in qualitative agreement (slightly lower) with the data reported by Elzanowska et al.[35] and Niki and Mizota.[36] The quantitative disagreement with the former data,[35] where acid-free working solutions were used, can be explained by errors in determining kinetic parameters (underestimation of the reduction rate) associated with hydrolysis of the Eu(III) complex in a solution of higher pH. The latter data[36] were obtained in working solutions with a high acid concentration which can cause slightly lower Eu(III) reduction rates due to the difference in ionic strength. The data obtained for the Cr(III) complex reduction are in qualitative agreement with data reported by Alias and Fawcett[11] for the case of a more acidic supporting electrolyte.

In the case of the supporting electrolyte with 0.03 M in $NaClO_4$ + 10^{-3} M $HClO_4$, the values of the rate constants for the reduction of Eu(III) found in the literature[14] are higher than the calculated ones. This can be associated with the fact that the analysis of the double layer effect on the reduction kinetics was performed in terms of an effective ϕ^d. If z_A is assumed to be +3, the potential at the reaction site was found to be 75%−85% of that at the oHp. This means that if the double layer effect is considered in terms of an effective charge, z_{eA} would be +2.25 to +2.55 (which is significantly lower than +3). Our study results in a similar conclusion.

Tafel plots corrected in accordance with the Gouy−Chapman model were first constructed using the Frumkin approach. In this case, ϕ^d was assumed to be equal to ϕ^d(GC). The resultant cTp values for integer reactant charges of +3 and +2 are presented in Figure 5. If z_A is assumed to be +3 (Figure 5b,d), the cTps for the two reactants in solutions with different concentrations of $NaClO_4$ do not overlap. Moreover, for $[Eu(H_2O)_n]^{3+}$, the slopes of these plots are significantly different (Figure 5d). However, when the ionic charge z_A is assumed to be +2, the cTp are closer to each other (Figure 5a,c). However, they still do not overlap well enough for both systems. For Cr(III), the Frumkin correction is overestimated using a formal charge of +2 (Figure 5a). Previously,[6] the fact that better agreement with experiment is found with a charge of +2 was attributed to ion pair association in the bulk of the solution. However, this may not be the only explanation of these observations as described below.

Effective charges for the reduced and oxidized forms of the chromium hexaaquacomplex and oxidized form of the europium hexaaquacomplex were calculated by using eqs 1 and 11 within the framework of the GC model and by using data for the interfacial potential distribution obtained by the MC data[7] (eqs 5, 8, 9, and 12). The model used to locate the reactant in the double layer is based on the idea that the center of charge of an ion cannot come right up to the electrode but is prevented from doing so not only by its own finite size but also by a solvation layer of solvent molecules (in this case, water) solvating the electrode. This model seems to be more realistic and self-consistent than the Gouy−Chapman model since it takes into account the size of the supporting electrolyte ions.

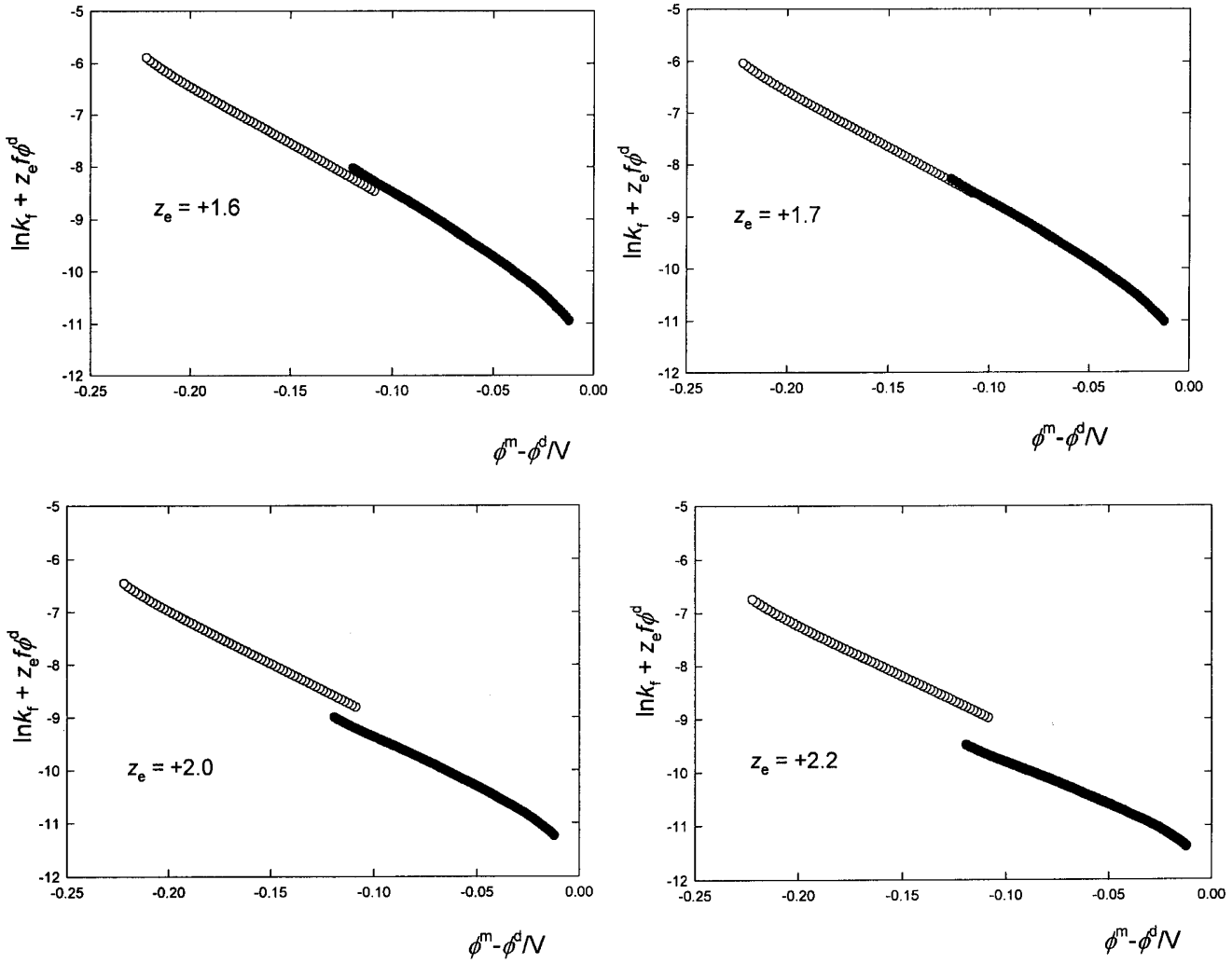

Figure 7. cTp for the reduction of $[Eu(H_2O)_n]^{3+}$ ions (5×10^{-4} M) in a solution of 0.3M $NaClO_4$ + 10^{-3} $HClO_4$ (open circles) and 0.03M $NaClO_4$ + 10^{-3} $HClO_4$ (solid circles) for different effective charges of the reacting complex as indicated.

The crucial point for this calculation is the choice of the distance of closest approach of the reactant. At this stage we assume that the reactant does not penetrate the inner layer but that it is located completely in the diffuse layer. For proper comparison of the results obtained using the two models, it is assumed that the distance of closest approach of the nearest atom of the reacting complex is located 100 pm from the oHp. This shift can be interpreted as a separation of the reactant and oHp by the secondary solvation shell of the reactant. Although the choice of reactant location is arbitrary, the two aquacomplexes are expected to be in similar locations in the double layer because they react at similar electrode charge densities.

The values of z_e obtained using the quantum chemistry data are presented in Table 2 parts a and b. Similar values of z_e for the Eu(III) aquacomplex were obtained for the number of ligands $n = 6$ and 8, and for differently oriented complexes with respect to the electrode surface; the result reported in the table is an average. It was noted that calculations based on the two models give essentially identical values for z_{Ae} and z_{Be} because the interfacial potential profiles in the case of 1−1 supporting electrolytes for the potential region under consideration differ very little. But this is not a general result and the results could be quite different, for example, in the case of 2−1 electrolytes.[7]

Parts a and b of Table 2 demonstrate that the effective charge of the Eu(III) aquacomplexes is less positive than that of the Cr(III) aquacomplex. This main result does not depend on our assumption about the number of ligands for the Eu(III) aquacomplex. The differences between z_{Ae} values for Cr(III) and Eu(III) aquacomplexes are almost identical (∼0.25) for both supporting electrolytes. In addition, it was found to be hardly at all affected by the reactant orientation and location with respect to the electrode. The final estimates for the z_e values can be affected by the choice of the potential distribution pattern. We believe that the corresponding overestimation of z_{Ae} is much higher for more dilute solutions. However, the relative values determined and the qualitative tendencies are more reliable than the absolute values.

Figures 6 and 7 present the evolution of the cTps for the reduction of $[Cr(H_2O)_6]^{3+}$ and $[Eu(H_2O)_n]^{3+}$ ions in the concentrated solution (0.3M $NaClO_4$) and dilute solution (0.03M $NaClO_4$) for different effective charges, z_e for the reactant. In the case of $[Cr(H_2O)_6]^{3+}$ reduction, when z_e increases from +2.0 to +2.2, the cTps approach each other; then at $z_e = +2.2$ they overlap but separate again for higher values of z_e. For reduction of $[Eu(H_2O)_6]^{3+}$ ion, the tendency is identical, but the cTps overlap for lower values of z_e, a result which was already predicted in the estimation of z_e (Table 2a,b).

In the above plots, the ordinate axis parameter was changed but the abscissa axis remained the same, namely, $\phi^m - \phi^d$. However, these plots are not completely self-consistent as is shown below by using data for Cr(III) reduction.

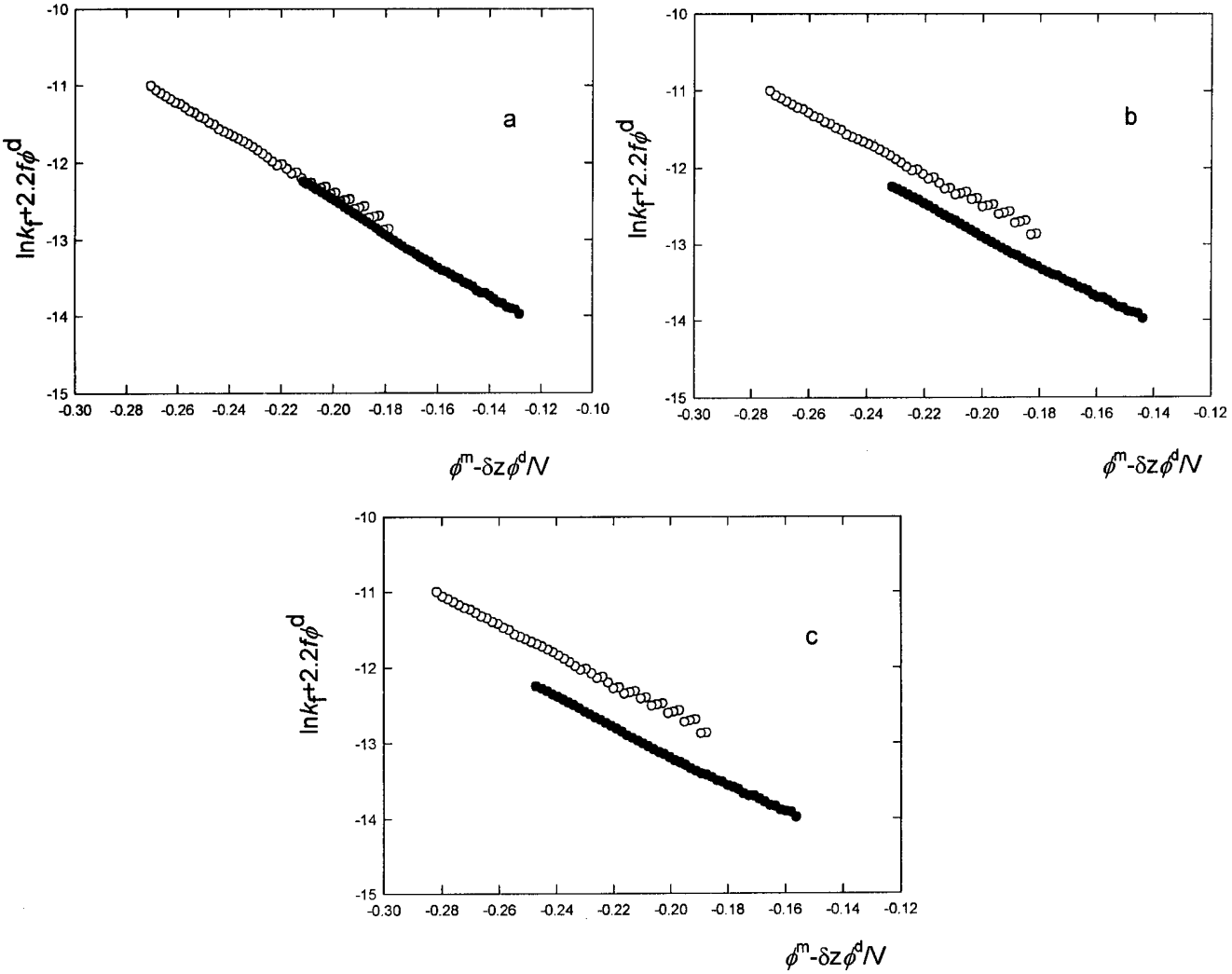

Figure 8. Corrected Tafel plots for the reduction of the $[Cr(H_2O)_6]^{3+}$ ions (5×10^{-4} M) in the concentrated (0.3 M, open circles) and diluted (0.03 M, solid circles) supporting electrolyte solutions with $z_e = +2.2$ and $\delta z = 0.68$ for the concentrated supporting electrolyte, and (a) $\delta z = 0.85$; (b) $\delta z = 0.6$; and (c) $\delta z = 0.4$ for the dilute solution where $\delta z = z_{Be} - z_{Ae}$.

TABLE 2: z_e for the Chromium Hexaaquacomplexes (Oxidized and Reduced Forms) and Europium Hexaaquacomplex (Oxidized Form)

σ^m, μC/cm^2	z_{Ae}/Cr(III)	z_{Ae}/Eu(III)	z_{Be}/Cr(II)	$z_{Ae} - z_{Be}$/Cr(III/II)
	a. In 0.3M $NaClO_4 + 10^{-3}$ M $HClO_4$			
−5	1.93	1.70	1.25	0.68
−10	1.94	1.70	1.25	0.69
	b. In 0.03M $NaClO_4 + 10^{-3}$ M $HClO_4$			
−5	2.56	2.30	1.71	0.85
−10	2.56	2.30	1.71	0.85

Consider now the potential dependence of the rate constant for the forward reduction reaction which is given by the equation

$$\ln k_f = \ln k_{fo} - w_A/RT - \alpha(F\phi^m - w_A + w_B)/RT \quad (14)$$

where w_A and w_B are the work terms associated with bringing the reactant and product to their reaction sites in the double layer, k_{fo} is the value of the forward rate constant at $\phi^m = 0$ and α is the transfer coefficient. Generally, the correction for the potential on the abscissa axis of the cTp is determined by the difference between w_A and w_B. Under these circumstances, cTps with $\phi^m - \phi^d$ as the abscissa variable are strictly speaking only correct if the charges z_A and z_B are integers, and their difference corresponds to the number of electrons transferred in the reaction. In the framework of the present molecular level approach, these conditions are not necessarily met so that the construction of an adequate cTp should involve reconsideration of eq 14.

Expressing w_A and w_B using the charges z_A and z_B, one writes

$$w_A = z_A F\phi^d \quad (15)$$

and

$$w_B = z_B F\phi^d \quad (16)$$

Substituting eqs 15 and 16 into eq 14, one may emphasize this point by writing

$$\ln k_f + z_A f\phi^d = \ln k_{fo} - \alpha f[\phi^m - (z_A - z_B)\,\phi^d] \quad (17)$$

It can be seen from Table 2a,b that for more realistic effective charges for the reactant and product, the difference $\delta z = (z_{Ae} - z_{Be})$ is not equal to unity. Thus, a more reasonable approach to construction of the cTp would be to use $\phi^m - (z_{Ae} - z_{Be})\phi^d$ as the abscissa variable.

A set of cTps for the reduction of $[Cr(H_2O)_6]^{3+}$ in the dilute and more concentrated electrolyte solutions constructed using the approach just described is presented in Figure 8. The z_{Be} and z_{Ae} values were determined by the quantum chemical calculations described earlier (Table 2a,b, last column). In this

case, we avoid using the z_{Ae} values for the dilute solutions which are most probably too large, and use $z_{Ae} = +2.2$ for which the corresponding cTps overlap. It was found that for case a in Figure 8, where the value of δz is the result of the quantum chemical calculations for $z_{Ae} - z_{Be}$, the cTps overlap perfectly. This implies that the present approach can be applied for cTp construction for the case that supporting electrolytes are used. However, the cTp do not overlap if z_{Ae} and z_{Be} obtained by the quantum chemical calculations (Table 2a,b) are used to estimate the value of the ordinate axis, This is undoubtedly associated with error in determining the reacting site potential (and z_{Ae} and z_{Be}) in the case of dilute supporting electrolytes. When the solution is more dilute, the local potential changes more rapidly with position so that the assumptions about reactant location are more important. Moreover, the fact that $\delta z \neq 1$ is of minor importance in this case. In the case of analysis of kinetic data for reactants with an asymmetrical distribution of charge this effect may play a more significant role in the constructing of cTps.

Conclusion

For the construction of cTps for real reactants with a size comparable with the thickness of the diffuse part of the double layer, the charge distribution within the reactant and product should be taken into consideration. Experimental results obtained in this work confirm the correctness of the approach developed by Tsirlina et al.[3] for cTp construction with consideration of a model reactant presented as a set of distributed local charges in terms of the effective potential at the reaction site.

It should be noted that both construction of z_e-based cTps and the quantum chemical calculations give a lower value of z_{Ae} for the europium(III) complex than for the chromium(III) one. This can be explained by the different electronic structures of the central atoms in the aquacomplexes. Having a smaller ionic radius, chromium ion exhibits a higher hydration energy and a less pronounced ability to form ionic associates, while for the bigger europium ion with a lower hydration energy, the effect of associated ligands on the resultant effective charge of the reacting species is more significant.

Results of the double layer effect on the reaction kinetics in the terms of effective charges of the species involved in the reaction are significantly affected by the model selected for the potential distribution in the vicinity of the electrode surface. For a 1−1 supporting electrolyte in the applicable region of electrode charge densities, both the GC and MC approaches were found to give similar patterns for the potential distribution. It is expected that for 2−1 supporting electrolytes, the MC approach would provide a more realistic description of the potential distibution which would be important in the construction of cTps.

Acknowledgment. W.R.F. acknowledges the hospitality of the Department of Electrochemistry of the Chemical Faculty of Moscow State University during a visit in which this manuscript was written. The financial support of the National Science Foundation, Washinton to W.R.F. is also gratefully acknowledged (CHE 0133758).

References and Notes

(1) Delahay, P. In *Double Layer and Electrode Kinetics*; John Wiley & Sons: New York, 1965.

(2) Frumkin, A. N.; Petry, O. A.; Nikolaeva-Fedorovich, N. V. *Electrochim. Acta* **1963**, *8*, 177.

(3) Tsirlina, G. A.; Petrii, O. A.; Kharkats, Y. I.; Kuznetsov, A. M. *Russ. J. Electrochem.* **1999**, *35*, 1210.

(4) Fawcett, W. R.; Hromadova, M.; Tsirlina, G. A.; Nazmutdinov, R. R. *J. Electroanal. Chem.* **2001**, *498*, 93.

(5) Tsirlina, G. A.; Petrii, O. A.; Nazmutdinov, R. R.; Glukhov, D. V. *Russ. J. Electrochem.* **2002**, *38*, 132.

(6) Hromadova, M.; Fawcett, W. R. *J. Phys. Chem. A* **2000**, *104*, 4356.

(7) Boda, D.; Fawcett, W. R.; Henderson, D.; Sokolowski, S. *J. Chem. Phys.* **2002**, *116*, 7170.

(8) Brynildson, M. E.; Bakac, A.; Espenson, J. H. *J. Am. Chem. Soc.* **1987**, *109*, 4579.

(9) Brynildson, M. E.; Bakac, A.; Espenson, J. H. *Inorg. Chem.* **1988**, *27*, 2592.

(10) Sellers, R. M.; Simic, M. G. *J. Am. Chem. Soc.* **1976**, *98*, 6145.

(11) Alias, K.; Fawcett, W. R. *Can. J. Chem.* **1974**, *52*, 3165.

(12) Anson, F. C.; Rathjen, N.; Frisbee, R. D. *J. Electrochem. Soc.* **1970**, *117*, 477.

(13) Yudi, L. M.; Baruzzi, A. M.; Solis, V. M. *J. Appl. Electrochem.* **1988**, *18*, 417.

(14) Gierst, L.; Cornellisen, P. *Collect. Czech. Chem Commun.* **1960**, *25*, 3004.

(15) Lyklema, J.; Parsons, R. *Electrical Properties of Interfaces—Compilation of Data on the Electric Double Layer on Mercury Electrodes*; U.S. Department of Commerce, National Bureou of Standards, Office of Standard Reference Data: Washington, DC, 1983.

(16) Bard, A. J.; Faulkner, L. R. In *Electrochemical Methods. Fundamentals and Applications*; 1980; p 237.

(17) Imbeaux, J. C.; Saveant, J. M. *J. Electroanal. Chem.* **1973**, *44*, 169.

(18) Saveant, J. M.; Tessier, D. J. *J. Electroanal. Chem.* **1975**, *65*, 57.

(19) Becke, A. D. *J. Chem. Phys.* **1992**, *98*, 372.

(20) Bol, W.; Welzen, T. *Chem. Phys. Lett.* **1977**, *49*, 189.

(21) Hay, P. J.; Wadt, W. R. *J. Chem. Phys.* **1985**, *82*, *270*.

(22) Habenschuss, A.; Spedding, F. H. *J. Chem. Phys.* **1980**, *73*, 442.

(23) Danielewicz-Ferchmin, I. *J. Phys. Chem.* **1995**, *99*, 5658.

(24) Marcus, Y. *J. Chem. Soc., Faraday Trans.* **1991**, *87*, 2995.

(25) Joubert, L.; Maldivi, P. *J. Phys. Chem.* **2001**, *105*, 9068.

(26) HyperChem. Computational Chemistry. Hypercube, Inc., 2002.

(27) Kowall, T.; Foglia, F.; Helm, L.; Merbach, A. E. *J. Phys. Chem.* **1995**, *99*, 13078.

(28) Cundari, T. R.; Stevens, W. J. *J. Chem. Phys.* **1993**, *98*, 5555.

(29) Gaussian 98, Revision A.11.2. Frisch, M. J.; Trucks, G. W.; Schlegel, H. B.; Scuseria, G. E.; Robb, M. A.; Cheeseman, J. R.; Zakrzewski, V. G.; Montgomery, J. A., Jr.; Stratmann, R. E.; Burant, J. C.; Dapprich, S.; Millam, J. M.; Daniels, A. D.; Kudin, K. N.; Strain, M. C.; Farkas, O.; Tomasi, J.; Barone, V.; Cossi, M.; Cammi, R.; Mennucci, B.; Pomelli, C.; Adamo, C.; Clifford, S.; Ochterski, J.; Petersson, G. A.; Ayala, P. Y.; Cui, Q.; Morokuma, K.; Rega, N.; Salvador, P.; Dannenberg, J. J.; Malick, D. K.; Rabuck, A. D.; Raghavachari, K.; Foresman, J. B.; Cioslowski, J.; Ortiz, J. V.; Baboul, A. G.; Stefanov, B. B.; Liu, G.; Liashenko, A.; Piskorz, P.; Komaromi, I.; Gomperts, R.; Martin, R. L.; Fox, D. J.; Keith, T.; Al-Laham, M. A.; Peng, C. Y.; Nanayakkara, A.; Challacombe, M.; Gill, P. M. W.; Johnson, B.; Chen, W.; Wong, M. W.; Andres, J. L.; Gonzalez, C.; Head-Gordon, M.; Replogle, E. S.; Pople, J. A. Gaussian, Inc., Pittsburgh, PA, 2001.

(30) Breneman, C. M.; Wieberg, K. B. *J. Comput. Chem.* **1990**, *11*, 361.

(31) Fawcett, W. R.; Smagala, T. G. *J. Phys. Chem.* **2004**, submitted.

(32) Fawcett, W. R.; Henderson, D. J. *J. Phys. Chem. B*, **2000**, *104*, 6837.

(33) Fawcett, W. R. *Russ. J. Electrochem.* **2002**, *38*, 2.

(34) Weaver, M. J.; Anson, F. C.*J. Electroanal. Chem.* **1975**, *65*, 711.

(35) Elzanowska, H.; Galus, Z.; Borkowska, Z. *J. Electrianal. Chem.* **1983**, *157*, 251.

(36) Niki, K.; Mizota, H. *J. Electroanal. Chem.* **1976**, *72*, 307.